Contents

1 Introduction

Because of its shallow root system, high water needs and drought sensitivity, potatoes often need irrigation in dry weeks (van Loon, 1981; Allen et al., 1998). It is indeed essential to avoid low tuber yield and loss tuber quality (Steduto et al., 2012). Additional water supply is even more useful in case of sandy soil, having a high hydraulic conductivity associated with low water storage capacity (Hartge et al., 2016). Associated with an adequate supply of nitrogen, a 40 ton/ha potato yield in Europe can be reached (Pot, 2015) (For early potato such as Amora, Sinora, Anosta and Première). On the other hand, a ridge plant system is used to avoid water pounding, aerate the soil (Tisdall and Hodgson, 1990) (van Loon, 1981), facilitate harvesting. Co-scheduling and estimation of the water and nitrogen needs is therefore complex, sometimes resulting in over-fertilization and a decrease of water and nitrogen efficiencies (Errebhi et al., 1998; Grizzetti et al., 2011). A better understanding of the water fluxes within this micro-topography is therefore essential. Nevertheless, measurement of these fluxes with classical point sensors is difficult due to the heterogeneity created by the microtopography of ridges and furrows and the associated processes.

Mathematical models have been developed recently to better understand water and solute movement within this specific micro-topography. Duncan et al. (2018) recently showed that solute leaching caused by pounding is reduced when roots are present in ridge plant systems under rainfall conditions. Ebrahimian et al. (2013) calculated that alternate furrow irrigation (irrigate one furrow in two, a system used in arid and semi-arid regions) could increase water and fertilizer efficiencies. Nevertheless, studies trying to measure these processes in temperate regions are contradictory. On one hand, (Saffigna et al., 1976) used dye tracing to show that stemflow induces a specific infiltration pattern directly in the ridge. On the other hand, Starr et al. (2005) proved that soil water fluctuation in the middle of the ridge were undetectable in the case of sprinkler irrigation for an amount of water applied varying ranging from 2.5 to 13mm. They used classical time-domain reflectometry (TDR) sensors for their study. Both studies were conducted in a loamy sand with sprinkler-irrigated potatoes (*Solanum tuberusom*).

A solution to overcome the lack of validation of model simulations, the lack of spatial coverage of point sensors and the lack of monitoring capacity in case of dye tracing is the use of non-invasive geophysical measurement techniques, such as electrical resistivity tomography (ERT). Electrical resistivity tomography provides spatio-temporal monitoring. This specific microtopography is typically subject to erosion during the growing season. One issue in the application of ERT, and more specifically the inversion of ERT data, is the effect of this poorly known topography on the obtained bulk resistivity distributions (Tong and Yang, 1990; Tsourlos et al., 1999; Garré et al., 2012). Rücker et al. (2006) compared the geometric factor for increasing electrode spacing without incorporation of the topography in the model. They showed that this resulted in artefacts in the resistivity distribution and concluded that the topography has to be incorporated correctly in the forward modelling mesh when the geometric effect is above 10%. Günther et al. (2006) then developed a method to incorporate arbitrary topography in the inversion scheme using cells to represent the model domain with topography.

Given the small resolution (i.e. small electrode distance) required to monitor water infiltration and uptake in ridge-furrow systems for potatoe, the topography effect could have a large effect. The objective of this study was therefore twofold: (1) to evaluate the effect of changes in surface microtopography in furrow-ridge potatoe systems on the quality of bulk resistivity distributions obtained with ERT and (2) to monitor the non-uniform infiltration pattern after an irrigation event on a sandy soil cropped with potato.

2 Material and method

2.1 Electrical resistivity tomography: measurement principle and data processing

In this study, we used 2.5D electrical resistivity tomography in a virtual and a real experiment. For such measurements, electrodes are inserted in the soil surface along a transect with a regular spacing. Direct current (DC) is injected between two electrodes and then the voltage is measured between two other electrodes. This is repeated for many different current and potential dipole combinations. The geometry of these combinations can vary and the different combinations have specific names (e.g. Wenner, dipole-dipole, ...) and properties (sensitivity and resolution). The selected combinations of dipoles in the measurement is called the electrode array.

In the virtual experiment, we tested the performance of various electrode arrays. To do this, we conducted a forward modelling step in which the total potential is computed with the different Poisson equations and mixed-boundary conditions (Dey and Morrison, 1979; Rücker et al., 2006; Ronczka et al., 2015) :

$$\nabla \times (\sigma \nabla(u)) = -\nabla.j \ in \ \Omega \tag{1}$$

$$\sigma(\frac{\partial u}{\partial n} + \beta u) = j.n \ on \ \partial\Omega \tag{2}$$

Equations (1) and (2) govern the potential $u(r)$ at a given location r with a conductivity distribution $\sigma(r)$, as a consequence of the current density j in the domain Ω and in its boundary $\partial\Omega$. The point electrode model (PEM) is then used to represent electrodes r_s with a singular current density function : $j = \delta(r - r_s)$. Rücker and Günther (2011) and Ronczka et al. (2015) have shown that this approximation should be handled with care in case of small electrode spacing. Evaluating the electrode effect is not part of the scope of this study, but is relevant for future work.. A finite-element method using unstructured triangle cells is used to solve equations (1) and (2) (Rücker et al., 2006).

Both the virtual as real ERT were inverted using a Gauss-Newton scheme with global regularization (Günther et al., 2006) to retrieve the resistivity distribution from the measured resistances using a regularization parameter λ, determining the smoothness level (Tikhonov and Arsenin, 1977).

$$\Phi = D \parallel (d - f(m)) \parallel_2^2 + \lambda \parallel C(m - m^0) \parallel_2^2 \rightarrow min \tag{3}$$

where D is the data weighting matrix, d is the vector containing the data, $f(m)$ is the model response, λ is the regularization parameter, C is the constraint matrix, m the model and m^0 a homogeneous reference model.

We used the fitted petrophysical relation for sand from Werban et al. (2008) to transform the resistivity (ρ) into a volumetric water content (θ).

$$ln(\rho) = -1.2 * ln(\theta) + 3.35 \tag{4}$$

2.2 Evaluation of performance and robustness of different electrode arrays in case of changing microtopography

After obtaining the soil moisture distribution using HYDRUS 2D/3D (Šimunek et al., 2018) converted it to a bulk resistivity distribution using a pedophysical relationship obtained from the literature (Cf. equation (4)). We performed virtual ERT measurement in this resistivity distribution using different arrays with the open-source library pyGIMLI (Rücker et al., 2017). After applying a random error, we inverted our apparent resistivity without incorporation of the micro-topography change using BERT (Günther et al., 2006). This procedure allowed us to evaluation to which extent uncertainty about the microtopography may induce errors in the ERT inversion result, knowing that they superpose to other known error sources of ERT such as smoothing due to the regularization and the ill-posedness of the inversion problem.

2.2.1 Hydrological model simulations

The soil-plant system in the soil hydraulic model Hydrus2D was designed to represent a typical field on a sandy soil in Flanders, Belgium. The soil had two main horizons : a loamy sand in the first 50 centimeter above 1.50 meter of pure sand. The ridge plant system (Cfr. figure 1) was composed of ridges with 20 cm height, repeated every 70 cm. The simulated domain contained six series of ridge-furrows computed for a total width of 4.05m with a depth of 2m. The soil hydraulic properties were based on a water retention curve from a field (Nearby Ten Aard) to compute Van Genuchten parameters using RETC for the loamy sand horizon. For the sand horizon, we used the ROSETTA database to predict the Van Genuchten parameters.

Table 1: Soil hydraulic parameters for van Genuchten relationship for both soil horizons.

	Loamy sand (0 to -0.5m)	Sand (-0.5m to -2m)
$\theta_R[-]$	0.01982	0.045
$\theta_S[-]$	0.5	0.43
$\alpha[1/cm]$	0.0173	0.145
$n[-]$	1.56	2.68
$l[-]$	0.5	0.5
$Ks[cm/hour]$	106	712

The imposed surface water flux during the spin-up (0 to 59 DAP) period was composed of rainfall and ET0 data obtained from the IRM meteorological station in Deurne (01/04/2017 - 29/05/2017). We applied a uniform atmospheric BC all over the surface. No root growth or root distribution is taken into account.

After this, we implemented root water uptake (**P2**) during 9 days (60 to 69 DAP) with a root distribution using the Vrugt equation (Vrugt and Hopmans, 2001), with transpiration values computed using Aquacrop (Steduto et al., 2009) and meteorological data from the Deurne station (31/05/2017 - 01/06/2017. We used values from Ahmadi et al. (2011) to have an estimation about a possible root distribution (Maximum root depth and depth of maximum intensity were taken at 50cm and 15cm below ridge surface). We implemented the Feddes model (Feddes et al., 1978) to modify the RWU regarding the available water content with the following parameters : P0 = -10cm, Popt = -25cm, P2H = -320cm, P2L = -600cm, P3 = -16000, r2H = 0.5 cm/day, r2L = 0.1 cm/day, values coming from (Wesseling, 1991).

Finally, we simulated a non-uniform infiltration pattern after an irrigation event. We assumed a canopy interception of 36% with 2.5 cm of water irrigated during one hour corresponding to an irrigation event as described by Saffigna et al. (1976). In our model, we simulated a crop stage corresponding to tuberization, i.e. 70 DAP. This is because water stress is particularly problematic during this period and therefore irrigation is relevant at this growing stage.(Miller and Martin, 1987; MacKerron and Jefferies, 1986).

We represented three different fluxes : F_1 (9.9cm) representing stemflow, in other words, the water intercepted by canopy and flowing to the main stem, as showed by (Saffigna et al., 1976). The canopy interception (C_i) was set to 36% with an interception length (L_i) on the entire ridge (55cm). We also decided a 5cm width for stemflow (L_s) at the top of the ridge (Cfr. figure 1 c).

$$F_1 = I * C_i * \frac{L_i}{L_s} \tag{5}$$

The water not intercepted but flowing trough the canopy and reaching the soil at the end, was assumed as uniformly distributed. This flux is named $F2$ (1.76cm) in the model and described below.

$$F_2 = I * C_i * \frac{L_i}{L_i - L_s} \tag{6}$$

Finally, F_3 (2.5cm) worth the water irrigated (I).
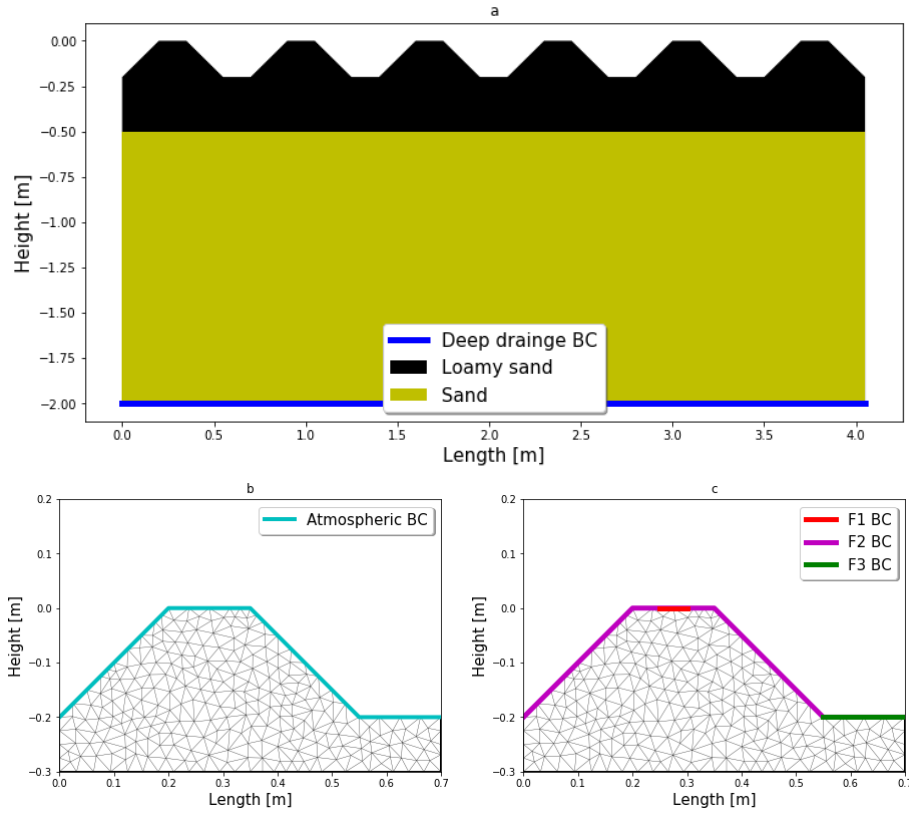
$$F_3 = I \tag{7}$$

Figure 1: Soil horizons and low boundary conditions for **P1,P2,P3** (a). Top BC for **P1** and **P2** (b). Top BC for **P3** (c).

2.2.2 Virtual ERT measurements and inversion

After computing the hydrological model, we conducted virtual ERT measures using different arrays based on different sensitivity distributions (Gaile et al., 2011) : Wenner-alpha (W-A), Dipôle-dipôle (DD), Pôle-dipôle (PD), and Dipôle-dipôle associated with a Wenner-alpha (WA+DD). ~~Each array was tested on different ridge height (0cm, -2cm, -4cm and -6cm) associated with different furrow depth (-20cm, -18cm, -16cm and -14cm).~~ We ~~considered~~ small electrodes of 13cm length represented ~~with points~~ located at 60% of their length : 7.8cm (Rücker and Günther, 2011). ~~Two electrodes were placed at the top of the ridge as in the furrows in addition with two more electrodes in each slope. With the resistivity change, we changed the PEM location at the top of the ridge and in the slope. Indeed, with the loss of material, the contact surface of the electrode was supposed smaller and therefore the representation of the electrodes had to be changed.~~ The forward modelling was computed with a 1% noise level having an absolute value of 1.10^{-6} The inversion was conducted with the initial mesh and PEM ~~(We stimulated an unknown micro-topography change)~~.

Since the microtopography is changing and the location of the electrodes stays the same, some electrodes are in areas where soil is disappearing and others in areas where soil is added. We therefore recalculated the 60 % of burried length for each electrode and each microtopography scenario for the forward modeling.
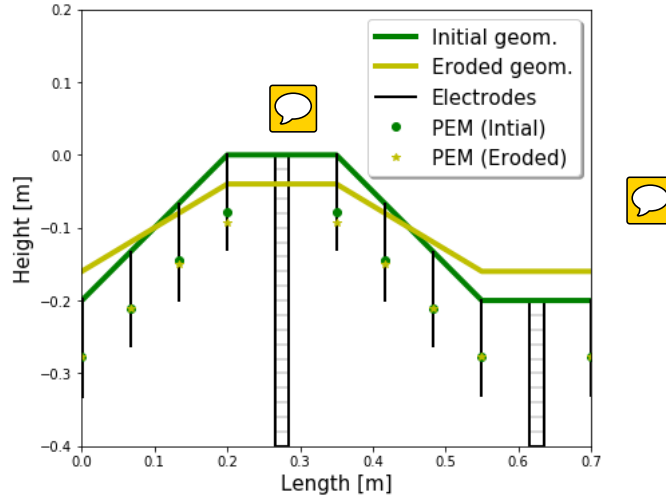
6

Figure 2: Initial and eroded mesh~~s~~ associated with their ~~PEM~~ locations. The eroded mesh is used for the forward modelling and the initial mesh for the inversion. The two ~~rectangular meshes correspond to the lines in the furrow and in the ridge used to have~~ 1-D water profile~~s~~

From the 2-D water content (WC) distribution, we extracted points representing the average of a 2cm by 2cm square to have a water profile in the furrow and in the ridge from 0 to -0.6m (Cfr. figure 4). We compared with the RMSE, line values from the model and from the inverted WC distribution to represent the error caused by the inversion, the array and the micro-topography change.

$$RMSE = \sqrt{\frac{\sum_{i=1}^{n}(WC_{Inverted,i} - WC_{Model,i})^2}{n}} \tag{8}$$

where n is the number of points compared between the model and the result of the inversion.

2.3 Monitoring non-uniform infiltration pattern in a potato field using ERT

Field measures were realised in the Campine region of Belgium, in Ten Aard (N 51°12.242′, E 4°57.522′). The potato crop was *Solanum tuberusom*, Zorba variety, planted the 15/04/2018. The sandy soil contained two main horizons : a first sandy horizon enriched in organic matter on the first 50 cm (from the top of the ridge) followed by a pure white sand horizon.

Figure 3: Soil horizons composed of a first sandy enriched in OM with a second white pure sand horizon.

ERT ~~line~~ was composed of 32 electrodes ~~distributed among 4 series of~~ ridges-furrows ~~as in the ERT design, geolocalized with the R10 GPS trimble.~~ ERT ~~measures~~ (Wenner-alpha) ~~have been achieved~~ with the MPT-DAS ~~(Each measure last 17min)~~. We also measured ~~with 5TE~~ temperature, conductivity and volumetric water content at 3 depths beneath one ridge (-20, -40 and -60cm) and at 2 depths beneath one furrow (-10 and -30 cm). One measure was taken before the irrigation (13/06/2018 at 7h10 = t0), another ~~measure was taken~~ just after the irrigation (13/06/2018 at 19h20 = t1) and finally ~~a last measure was taken just taken~~ one day after the irrigation (14/06/32018 at 16h10 = t2) . ~~In addition to the in-situ measures of the soil water system,~~ we ~~also~~ put 8 ~~small~~ rain gauges with a half-meter gap ~~regarding~~ the ERT line in the furrow and the ridge, to estimate canopy interception in the furrow/ridge during an irrigation event.
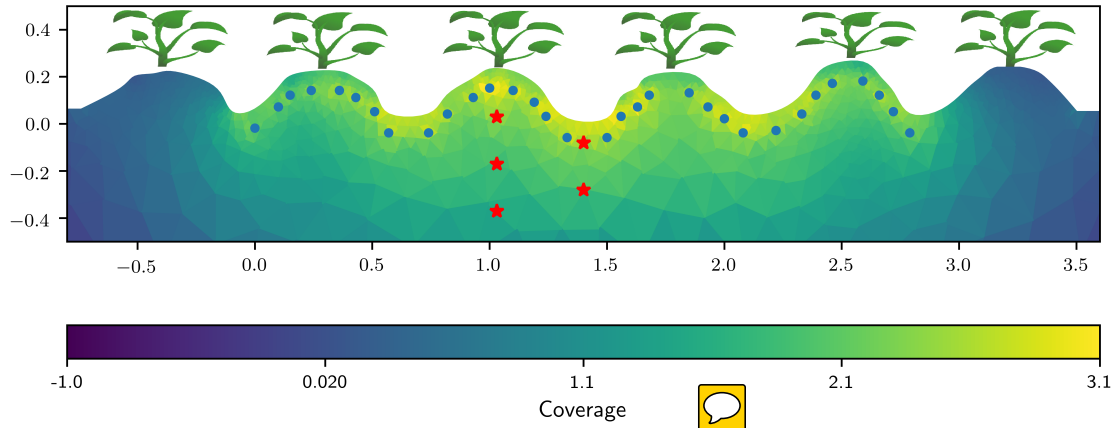

Figure 4: ERT transect with electrodes represented by blue dots. 5TE probes are represented by the red stars. Coverage is displayed on the 2-D transect.

8

3 Results and discussion

3.1 Performance and robustness of different electrode arrays

Recovery of the different arrays to an initial soil moisture pattern

Figure 5 and 6 show the 2-D hydrological model with the inverted WC distribution of the four arrays chosen (Wenner-a, Dipôle-dipôle, Pôle-dipôle and Wenner-a + Dipôle-dipôle). Figure 5 corresponds to the timeframe = 69 days, whereas the root water uptake was setted during the last ten days without rain. Figure 6 corresponds to the timeframe = 70 days, just after an non-uniform irrigation of 25mm. For both models, we distinguish the clear transition of WC between the two soil horizons (at -0.5m). Furthermore, despite the spin-up and the micro-topography, the models remain relatively homogeneous.

Concerning the inverted WC distribution, patterns from the Rwu (Figure 5) are mostly recovered by the W-a array despite an artefact just below each furrow inducing a high WC (more than 0.8 cm^3/cm^3 at -0.4m (For a graphical reason, we set-up the maximum values of the water content to 0.5, even if we know that at -0.4m below each furrow for the W-A, the WC goes until 0.8)). We can also see a wrong water decrease just below each furrow for the W-a (at -0.25m), that could come from the RWU bulb in the ridge or because of the compensation need coming from the WC increase at -0.4m. Nevertheless, the W-a is the only array without a wrong noisy water content distribution. Indeed, all the others arrays, despite the right water decrease at the top of the ridge have a highly noisy WC distibution that is not present in the model. We conclude that the W-a is the best array to reproduce pattern in the ridge caused by the Rwu.
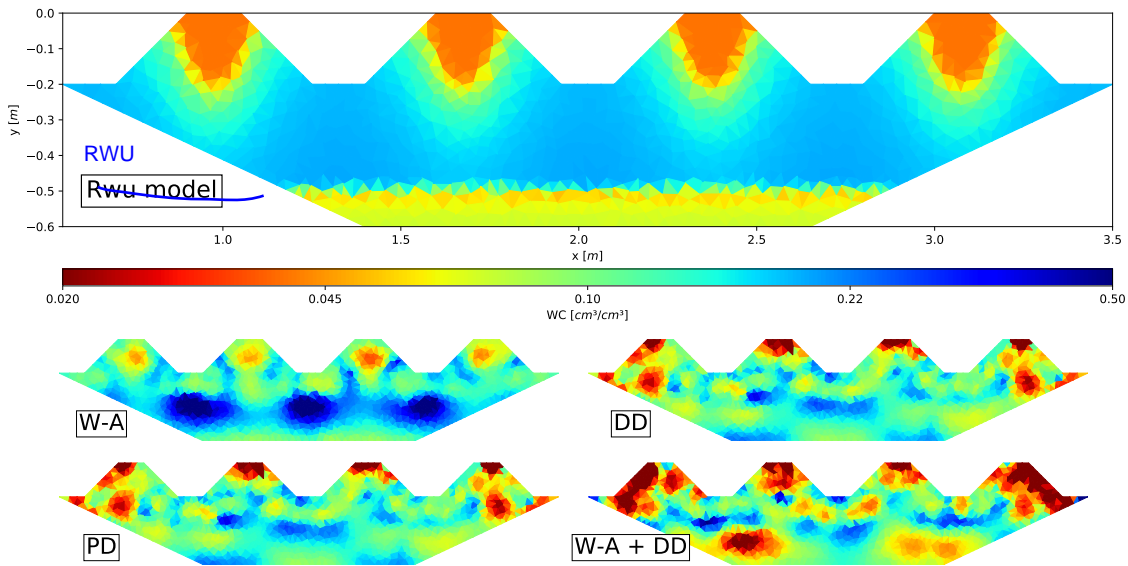

Figure 5: Root water uptake model associated with inverted resistivity of four arrays : Wenner-a (W-A), Dipôle-dipôle (DD), Pôle-dipôle (P-D) and Wenner-a + Dipôle-dipôle (W-A + DD) .

For the figure 6, in overall, the four arrays seem to better reproduce the intial model. This could come from a more homogeneous model but also because of the irrigation. Indeed, with the add of water, the subsoil surface is less resistive and therefore more sensitive to the current flow. Again, the W-a, with the Pôle-dipôle in this case, seem to recover the best the intial WC distribution even if the soil horizon transition is well smoothed. The DD and PD + W-a seem to have again a noisy 2-D, even more noticeable with the W-a + DD. The W-a is therefore the best array to reproduce pattern of Rwu and non-uniform infiltration patten.
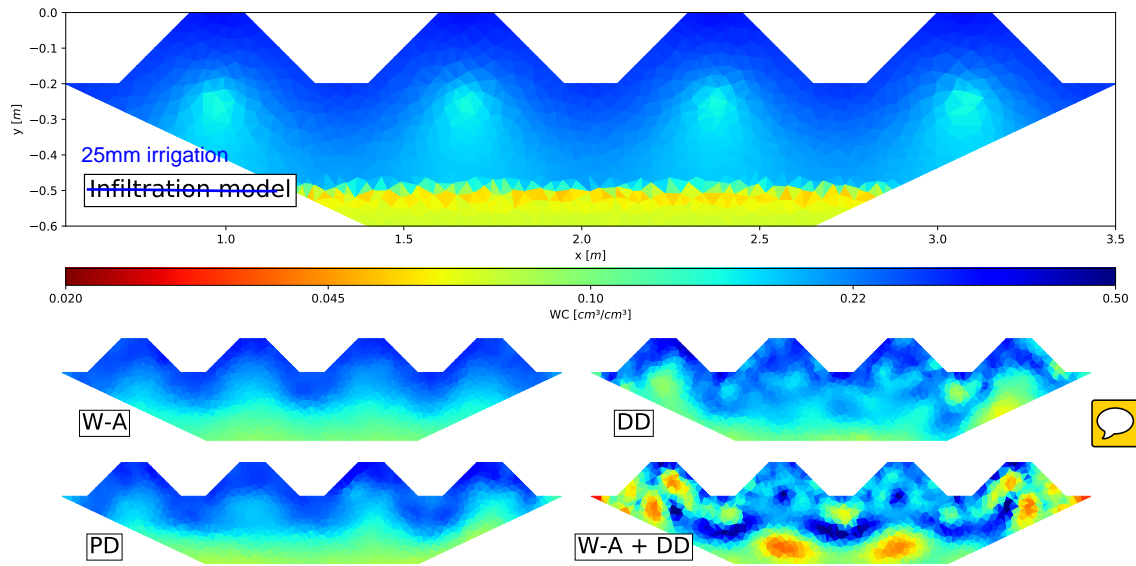
9

Figure 6: Infiltration model associated with inverted resistivity of four arrays : Wenner-a (W-A), Dipôle-dipôle (DD), Pôle-dipôle (P-D) and Wenner-a + Dipôle-dipôle (W-A + DD).

The one-dimensional water profiles (Figure 7) contain informations about the depth of the front infiltration or the Rwu bulb. ~~This graph is also useful to better distinguish water processes and artefacts produced by the inversion between ridges and furrows.~~ ~~We can fisrtly say that~~ the 1-D line in the furrow of the Rwu model is best reproduced by the PD. D-D and W-A + DD are quiet similar with a wrong WC decrease at -0.3m. As ~~seen~~ in ~~the~~ figure 5, ~~we distinguish~~ a ~~harsh~~ artefact ~~for~~ the W-A at -0.4m. The 1-D in the ridge of the Rwu of the W-A, despite a wrong small ondulation between -0.1 and -0.5 and a deeper RWu bulb, is the best array to retrieve the Rwu pattern. ~~The result of the three other arrays of the Rwu in the ridge give a wrong interpretation of the model. It is therefore important important to only use the W-A if we want to distinguish the Rwu bulb there.~~ The 1-D line in the ridge and the furrow of the infiltration model is well reproduced, despite a smoothing, by the W-A and the W-A and DD. The W-A + DD ~~gives again a complete wrong interpretation regarding the intial model.~~ ~~This is a first different conlusion with Garré et al. (2011) who proved that W-A + DD was the best array to reproduce soil moisture pattern in contour Hedgerow intercropping system (In that case, there was no micro-topography, but the models were more heterogeneous).~~

This shows the strong impact of the presence of microtopography and related error propagation in the inversion results.
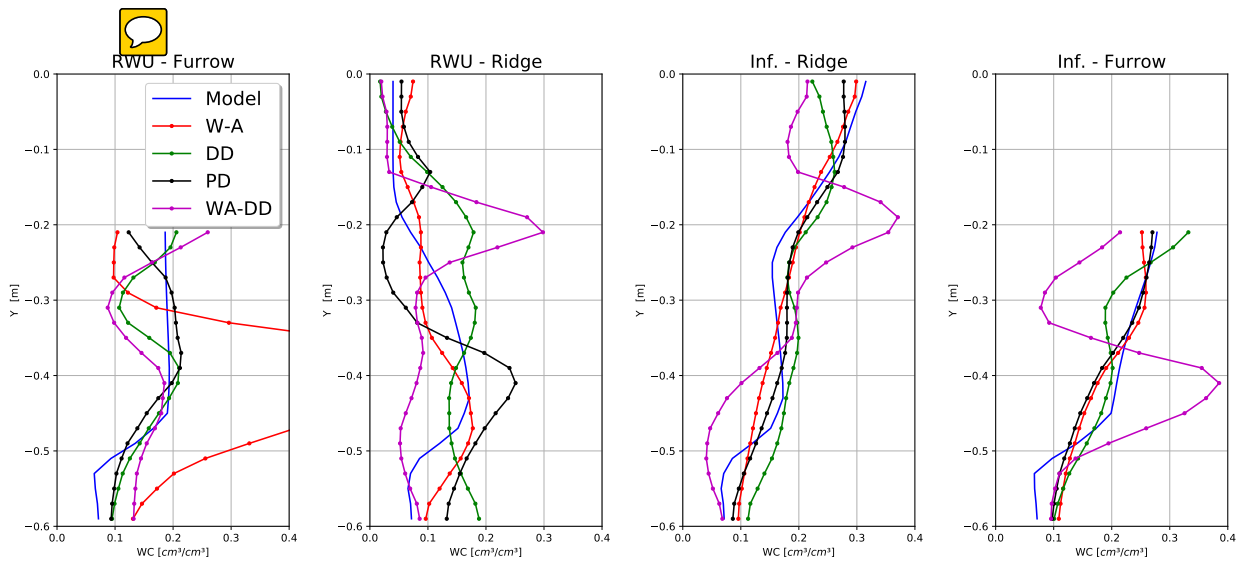
Figure 7: Water profile in the Root water uptake and Infiltration models associated with inverted resistivity without micro-topography change.

Table 2 represents the RMSE error between the model and the result of the inversion. We can firstly confirm that the WA is the best array to reproduce the non-uniform infiltration pattern (RMSE of 2.76 %). In the case of the Rwu model, the RMSE of the 2-D distribution is the highest (10.55 %) but because of the huge RMSE in the furrow (20.45 %) caused by the artefact in the furrow. We also know from figure 5 that patterns of the Rwu in the ridge were best reproduced with the W-A in the ridge (Confirmed with the low RMSE of the water profile in the ridge (3.45 %).

RMSE [%]		W-A	DD	PD	W-A+DD
	All	10.55	6.85	8.77	7.72
Rwu	Ridge	3.45	6.21	5.91	8.40
	Furrow	20.45	3.13	2.20	4.77
	All	2.76	5.18	3.01	10.34
Inf.	Ridge	2.35	4.12	2.06	8.54
	Furrow	2.41	2.88	2.22	8.92

Table 2: RMSE between the model and the result of the inversion without micro-topography change. All = RMSE of the 2-D WC distribution. Ridge = RMSE values between the 1-D line of the model and the 1-D line the inversion. Furrow = RMSE values between the 1-D line of the model and the 1-D line the inversion.

3.2 Effect of the micro-topography change on the Wenner-alpha array

~~We then choose the W-A as the best array to reproduce soil moisture pattern with a specific micro-topography. But during the growing season, we know that because of erosion, a possible micro-topography change can happen. We therefore checked the resilience of the W-A array to a micro-topography change.~~

Figure 8 represents the result of the inversion of the Rwu model with ~~a stimulated~~ the eroded mesh for the W-A array (Cfr. figure 4). Globally, the micro-topography change does not affect the location of the Rwu bulb, as with the non-eroded mesh (cfr. figure 5). All Rwu bulbs have a less important WC, excepted for the 18cm mesh. Also, artefacts beneath ridges are less important with the 18cm eroded mesh, which is not the case with the 14cm eroded mesh whereas wrong water increase appear again. We can then conclude that the location of the RWU bulb in the ridges can be retrieve with a micro-topography change with the W-A array.
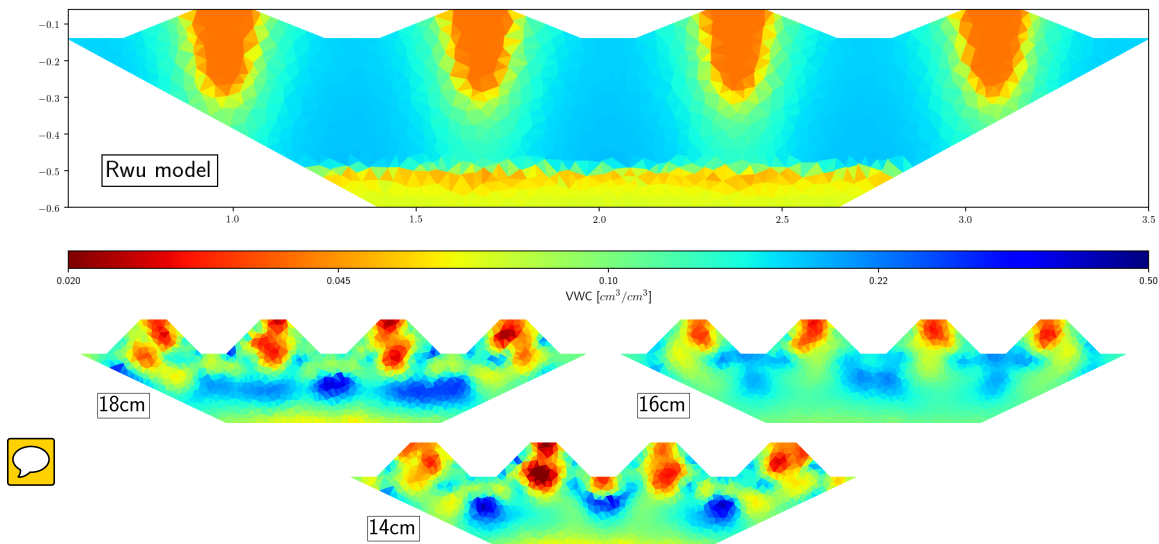
Figure 8: Infiltration model associated with inverted resistivity with a micro-topography change with the W-A array.

Water profile in the ridge and furrow confirm the resilience of the W-A array to the micro-topography change (Figure 9). Nevertheless, an important point needs to be notified with the infiltration model : WC at the top subsurface of the ridge and the furrow is under-estimated, especially in the ridge with high height decrease. The front is in fact moved down, accompanied with a WC decrease.
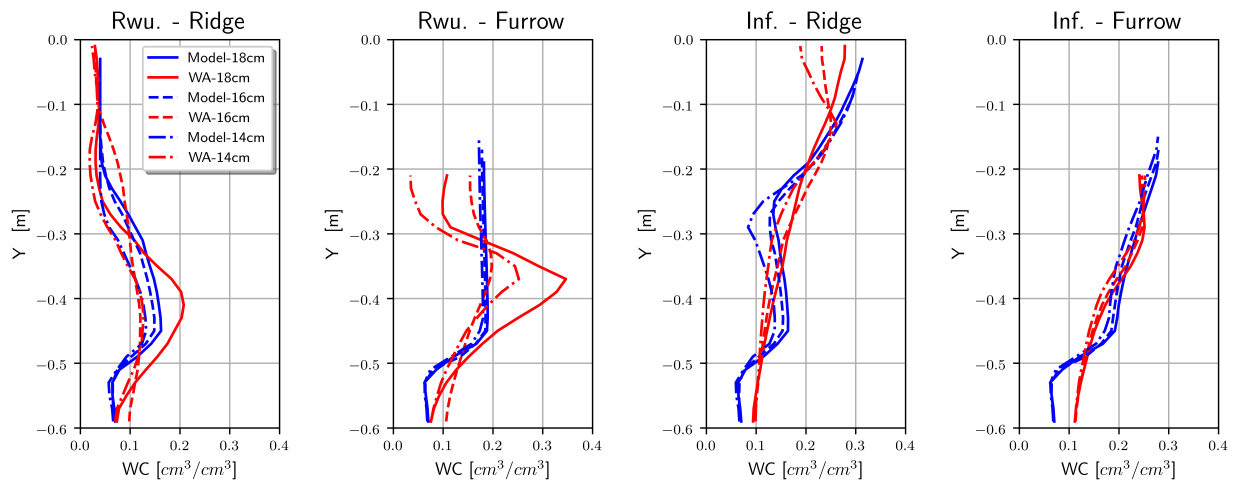

Figure 9: 1-D line in the Root water uptake (Rwu) and Infiltration (Inf.) models associated with inverted resistivity.

3.2 ₃ Soil moisture dynamic after an irrigation

5TE measures with correlation with ERT
- Graph with WC and temperature evolution from 5TE
- R^2 between ERT measures and 5TE

ERT measures

This should come after you showed 3.3.2 Resistivity distribution

The obtained resistivity distribution at t0 (before the irrigation), t1 (just after the irrigation) and t2 (one day after the irrigation) are represented in figure 10. Firstly, we distinguish clear

Rwu bulb (at t0) in the 4 ridges. We also see an important resistivity increase between the third and fourth ridge that could come from a water uptake directly in this furrow. We do not distinguish soil moisture change, even smoothed, with the horizon transition at -0.3m. Finally, beneath -0.40m, the resistivity seems to remain globally constant.
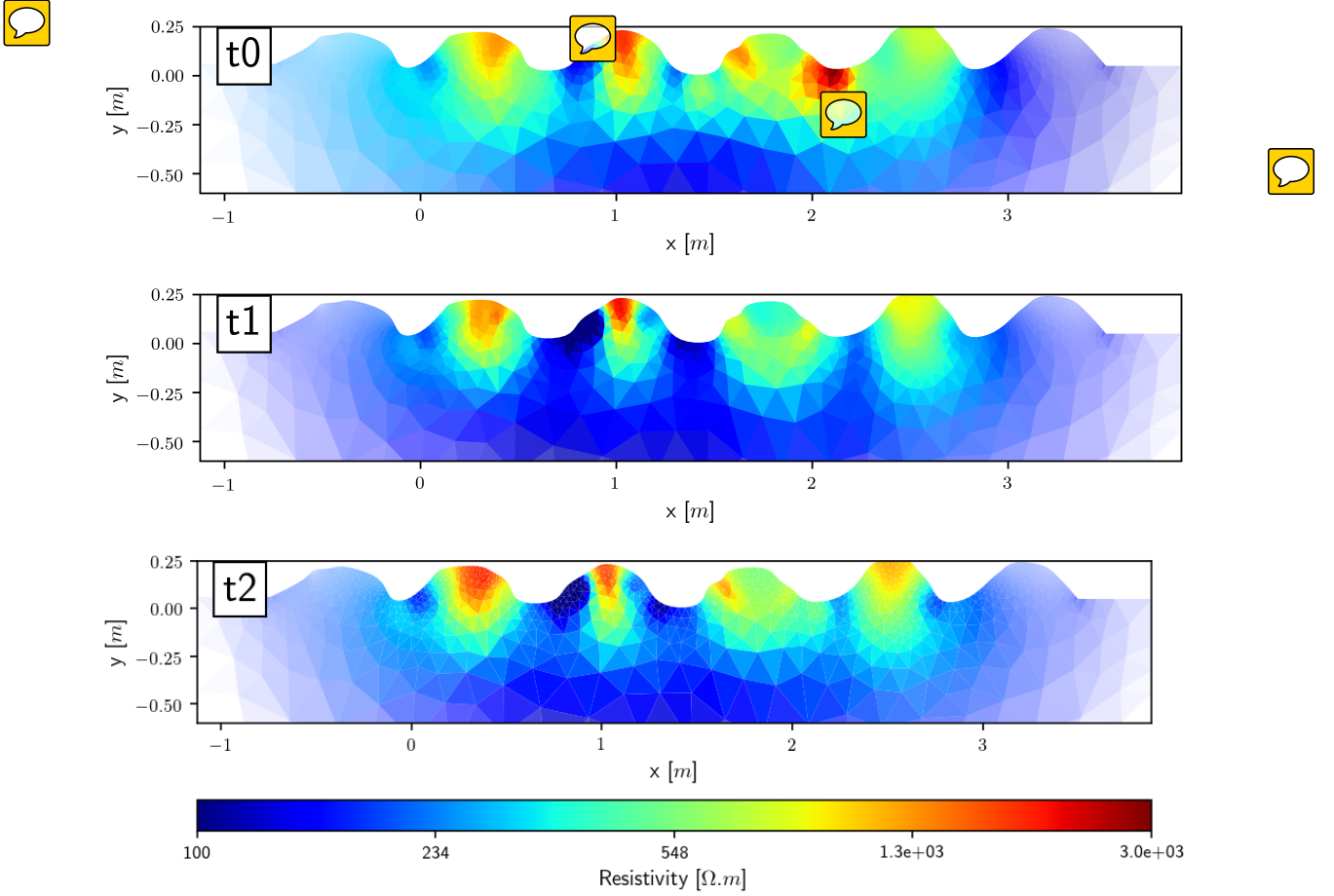

Figure 10: Resistivity distribution before the irrigation (13/06/2018 at 07h10 = t0), just after the irrigation (13/06/2018 at 19h10 = t1) and one day after the irrigation (14/06/2018 at 16h20 = t2).

3.2.3 Soil moisture dynamics and distribution from ERT

With the petrophysical relation (Cfr. equation (4)), we transformed the obtained bulk resistivity into a volumetric water content distribution to display WC differences between two time-steps (Figure 11). The first difference of WC (Δt_1) explains where do the irrigated water goes. We can firstly say that, in the three furrows covered by the ERT line, a major bulb infiltration (on the 15cm width of the three furrows) occur, explained by the non-interception (or less important than in the ridge) of the the canopy in the furrow, inducing a more important water increase. On the other hand, we do distinguish a slight WC increase in the third ridge, but not reproduced in others whereas the WC seems constant, This is firstly due by the interception percentage of the water that was really high. This could be also explained because during the day, just before the irrigation (between 7h10 and 19h), the WC continue to decrease, but could have been directly recovered by a small WC increase. The second water difference explains differences between WC distribution one day after the irrigation and just before the irrigation (Δt_2). We observe water decrease in furrows (-10%), however it's difficult to say if mainly because of evaporation or water uptake. We also see that the water added in the third ridge is also evapotranspirated.
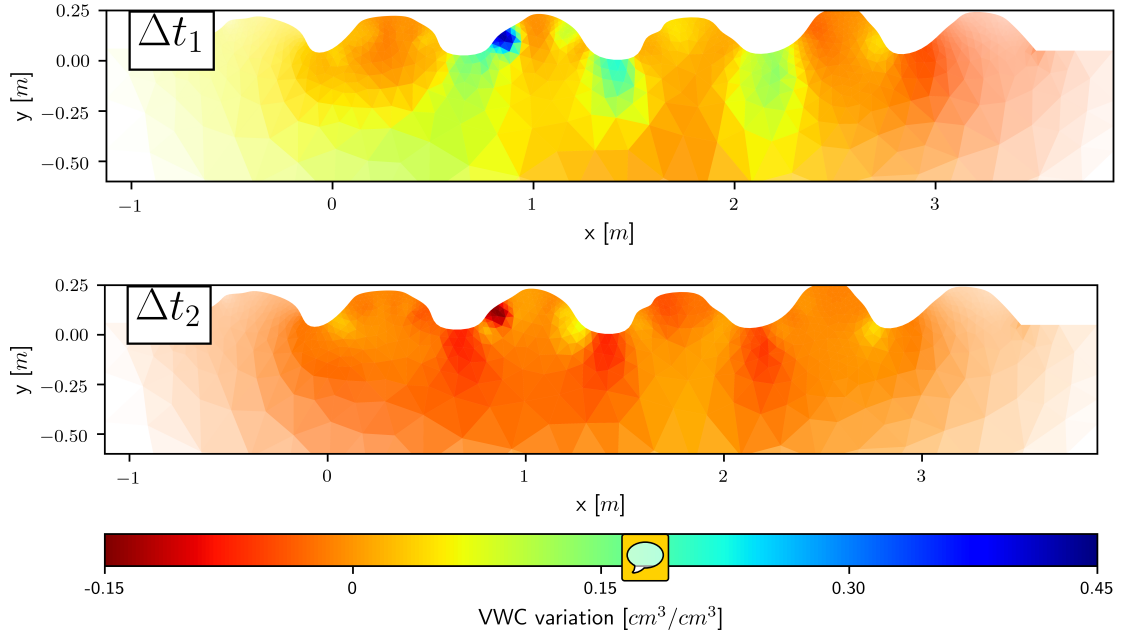
13

Figure 11: Water content variation before and after the irrigation (Δt_1) and one day after the irrigation minus just after the irrigation (Δt_2).

3.2.4 1-D soil water profiles in ridge and furrow

The 1-D water profiles (Figure 12) allow us to better distinguish water processes between furrows and ridges. In the first place, in ridges, we confirm evapo-transpiration until -0.2m whereas the concavity of the water profile changes at t0 (i.e. in the first 40cm of the subsurface). We also see this pattern in the furrow but with less significance (only in the first 20cm). Concerning the VWC variation in ridges, because of the high canopy interception, we only see $\pm$ 5% of VWC variation in the third ridge on the first 5 centimeter. We also see a water increase (from 5 to 10 %) from -0.3 to -0.6m beneath the third ridge, certainly because of water redistribution from furrows. Indeed, water increase is way more visible in furrows with more than 10% increase in the first 30 cm for the three furrows Δt_2. Half of this water ($\pm$ 5%) is then evapotranspirated the day after, always in the first 30 cm. We can then conclude and confirm the conclusion of (Starr et al., 2005), saying that water increase with Sprinkler irrigation was mainly in furrows without stemflow in ridges.
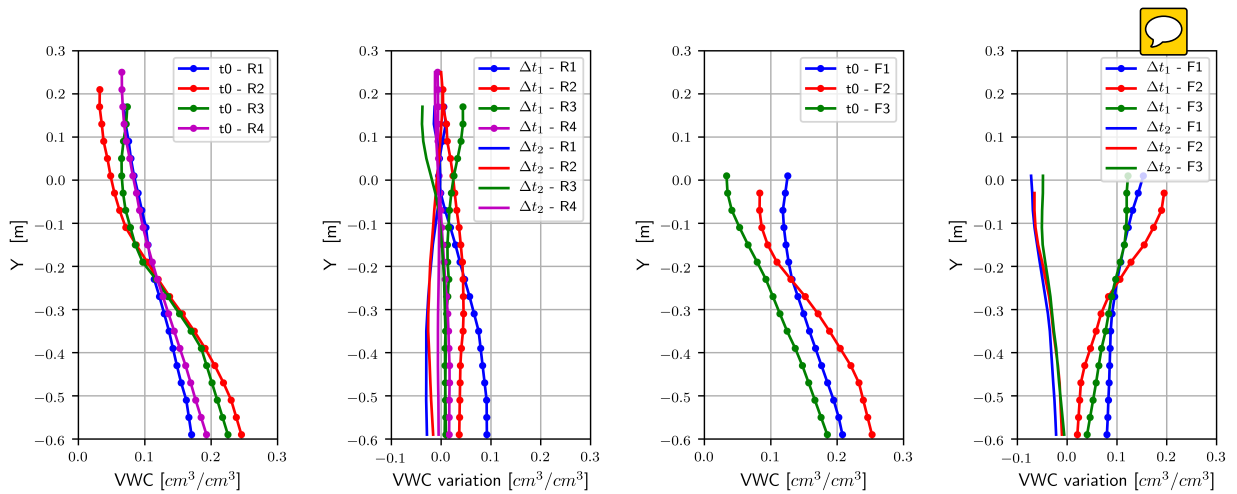

Figure 12: Water profiles in 4 ridges (R) and 3 furrows (F) of the intial WC distribution (t0), associated with timelapse measure (Δt_1 and Δt_2). Each point in the line corresponds to a 4cm length by 2cm width rectangle interpolated from the 2-D WC distribution.

3.2.5 Characterization of potato root system and efficiency of irrigation

14

3.3   Rain gauges measure

4   Conclusion

- Possible to retrieve soil moisture pattern with a specific micro-topography. - Infiltration front mainly in furrows.

References

(2015). POTENTIAL proposal.

Ahmadi, S. H., Plauborg, F., Andersen, M. N., Sepaskhah, A. R., Jensen, C. R., and Hansen, S. (2011). Effects of irrigation strategies and soils on field grown potatoes: Root distribution. *Agricultural Water Management*, 98(8):1280–1290.

Allen, R. G., Pereira, L. S., Raes, D., Smith, M., and Ab, W. (1998). Allen_FAO1998. pages 1–15.

Dey, A. and Morrison, H. F. (1979). RESISTIVITY MODELLING FOR ARBITRARILY SHAPED TWO-DIMENSIONAL STRUCTURES*. *Geophysical Prospecting*, 27(1):106–136.

Duncan, S. J., Daly, K. R., Sweeney, P., and Roose, T. (2018). Mathematical modelling of water and solute movement in ridge plant systems with dynamic ponding. *European Journal of Soil Science*, 69(2):265–278.

Ebrahimian, H., Liaghat, A., Parsinejad, M., Playán, E., Abbasi, F., and Navabian, M. (2013). Simulation of 1D surface and 2D subsurface water flow and nitrate transport in alternate and conventional furrow fertigation. *Irrigation Science*, 31(3):301–316.

Errebhi, M., Rosen, C. J., Gupta, S. C., and Birong, D. E. (1998). Potato Yield Response and Nitrate Leaching as Influenced by Nitrogen Management. *Agronomy Journal*, 90(1):10.

Feddes, R., Penning de Vries, F. W. T., and van. Laar, H. H. (1978). *Simulation of plant growth and crop production*. Centre for Agricultural Pub. and Documentation.

Garré, S., Coteur, I., Wongleecharoen, C., Kongkaew, T., Diels, J., and Vanderborght, J. (2012). Noninvasive Monitoring of Soil Water Dynamics in Mixed Cropping Systems: A Case Study in Ratchaburi Province, Thailand.

Garré, S., Günther, T., Diels, J., and Vanderborght, J. (2011). Evaluating Experimental Design of ERT for Soil Moisture Monitoring in Contour Hedgerow Intercropping Systems.

Grizzetti, B., Bouraoui, F., Billen, G., van Grinsven, H., Cardoso, A. C., Thieu, V., Garnier, J., Curtis, C., Howarth, R., and Johnes, P. (2011). Nitrogen as a threat to European water quality. *The European Nitrogen Assessment*, pages 379–404.

Günther, T., Rücker, C., and Spitzer, K. (2006). Three-dimensional modelling and inversion of dc resistivity data incorporating topography - II. Inversion. *Geophysical Journal International*, 166(2):495–505.

Hartge, K. H., Horn, R., Horn, R., Horton, R., Bachmann, J., and Peth, S. (2016). *Essential soil physics : an introduction to soil processes, functions, structure and mechanics*.

MacKerron, D. K. L. and Jefferies, R. A. (1986). The influence of early soil moisture stress on tuber numbers in potato. *Potato Research*, 29(3):299–312.

Miller, D. E. and Martin, M. W. (1987). Effect of declining or interrupted irrigation on yield and quality of three potato cultivars grown on sandy soil. *American Potato Journal*, 64(3):109–117.

Ronczka, M., Rücker, C., and Günther, T. (2015). Numerical study of long-electrode electric resistivity tomography — Accuracy, sensitivity, and resolution. *Geophysics*, 80(6):E317–E328.

Rücker, C. and Günther, T. (2011). The simulation of finite ERT electrodes using the complete electrode model. *Geophysics*, 76(4):F227–F238.

Rücker, C., Günther, T., and Spitzer, K. (2006). Three-dimensional modelling and inversion of dc resistivity data incorporating topography - I. Modelling. *Geophysical Journal International*, 166(2):495–505.

Rücker, C., Günther, T., and Wagner, F. M. (2017). pyGIMLi: An open-source library for modelling and inversion in geophysics. *Computers and Geosciences*, 109(July):106–123.

Saffigna, P. G., Tanner, C. B., and Keeney, D. R. (1976). Non-Uniform Infiltration Under Potato Canopies Caused by Interception, Stemflow, and Hilling. *Agronomy Journal*, 68(2):337.

Šimunek, J., Šejna, M., and Van Genuchten, M. T. (2018). New features of version 3 of the HYDRUS (2D/3D) computer software package. *Journal of Hydrology and Hydromechanics*, 66(2):133–142.

Starr, G. C., Cooley, E. T., Lowery, B., and Kelling, K. (2005). Soil water fluctuations in a loamy sand under irrigated potato. *Soil Science*, 170(2):77–89.

Steduto, P., Hsiao, T. C., Fereres, E., and Raes, D. (2012). *Crop yield response to water*.

Steduto, P., Hsiao, T. C., Raes, D., and Fereres, E. (2009). Aquacrop-the FAO crop model to simulate yield response to water: I. concepts and underlying principles. *Agronomy Journal*, 101(3):426–437.

Tikhonov, A. and Arsenin, V. Y. (1977). *Methods for solving ill-posed problems*. John Wiley and Sons, Inc.

Tisdall, J. and Hodgson, A. (1990). Ridge tillage in Australia: a review. *Soil and Tillage Research*, 18(2-3):127–144.

Tong, L. and Yang, C. (1990). Incorporation of topography into two-dimensional resistivity inversion. *GEOPHYSICS*, 55(3):354–361.

Tsourlos, P. I., Szymanski, J. E., and Tsokas, G. N. (1999). The effect of terrain topography on commonly used resistivity arrays. *GEOPHYSICS*, 64(5):1357–1363.

van Loon, C. D. (1981). The effect of water stress on potato growth, development, and yield. *American Potato Journal*, 58(1):51–69.

Vrugt, J. A. and Hopmans, J. W. (2001). Calibration of a Two-Dimensional Root Water Uptake Model. *Management*, 65(4).

Werban, U., Al Hagrey, S. A., and Rabbel, W. (2008). Monitoring of root-zone water content in the laboratory by 2D geoelectrical tomography. *Journal of Plant Nutrition and Soil Science*, 171(6):927–935.

Wesseling, J. (1991). Meerjarige simulatie van grondwaterstroming voor verschillende bodemprofielen, grondwatertrappen en gewassen met het model SWATRE. Technical report, Wageningen : DLO-Staring Centrum, Feddes_param.